Pergamon

Journal of Structural Geology, Vol. 17, No. 3, pp. 329 to 343, 1995

0191-8141/95 $9.50+0.00

0191-8141(94)00078-6

Vertical and fold-axis parallel extension within a slate belt in a transpressive setting, northern Appalachians

DONNA KIRKWOOD

Département de Géologie, Université Laval, Sainte-Foy (Québec), Canada, G1K 7P4

MICHEL MALO

INRS Géoressources CGQ, C.P. 7500, Sainte-Foy (Québec), Canada, G1V 4C7

and

PIERRE ST-JULIEN and PIERRE THERRIEN

Département de Géologie, Université Laval, Sainte-Foy (Québec), Canada, G1K 7P4

(*Received* 18 *August* 1993; *accepted in revised form* 5 *May* 1994)

Abstract—An incremental and finite strain study of a Mid-Paleozoic slate belt in a transpressive setting in Gaspé, Canadian Appalachians, has been undertaken using syntectonic fibers from pyrite-type pressure shadows. Regionally, strain estimates are quite consistent and reflect only slightly higher strain in the central part of the anticlinorial structure defining the slate belt. Extensions of up to 160% vertically and 110% parallel to the fold axis were recorded in the slate belt combined with an estimated overall regional shortening of 80%. The fibers first rotated toward the final position of the cleavage within a vertical section normal to the cleavage, and then rotated from a vertical to a horizontal orientation. This change in fiber orientation observed in cleavage-parallel sections indicates an abrupt change in the incremental stretching direction from sub-vertical to sub-horizontal (fold-axis parallel). The vertical extension is related to folding and cleavage development during coaxial flattening. The horizontal extension reflects the strain imposed on the rocks during regional simple shear which produced strike-slip faulting and further tightening of the folds. Folding, cleavage development, fold-axis parallel extension and faulting are all related to oblique convergence during the Middle Devonian Acadian orogeny in this part of the Canadian Appalachians and clearly indicate an overall transition from a pure shortening deformation to a simple shear dominant deformation in an overall transpressive setting.

INTRODUCTION

Rocks bordering fault zones in convergent wrench or transpressive systems are affected by both pure and simple shear (Sanderson & Marchini 1984). In such systems, shortening normal to the fault zone and transcurrent shear parallel to the fault zone bring about the development of folds, thrust faults and transcurrent faults. Development of folds occurs either before faulting (Lafrance 1989) or simultaneous with faulting in wrench settings (Richard *et al.* 1991). Such folds are subject to a component of shear strain (Sanderson & Marchini 1984), and kinematic models of transpressive terranes predict considerable axial extension and fold axis rotation (Bürgmann 1991, Jamison 1991). In pure wrench terranes, horizontal maximum extension and shortening directions are parallel to the major and minor strain ellipse axes, respectively (Wilcox *et al.* 1973). Our strain study was undertaken in order to determine the progressive deformation history of a Mid-Paleozoic slate belt within a transpressive setting, the Gaspé Trough. The belt is located within the boundary zone of an important strike-slip fault of the Gaspé Peninsula, the Grand Pabos-Restigouche fault (Fig. 1), in the Canadian Appalachians. Our data indicate that vertical extension associated with folding and cleavage development occurred prior to fold-axis parallel extension in the Gaspé Trough. The abrupt reorientation of the stretching axis, from subvertical to subhorizontal, records the transition from a pure shortening deformation to a simple shear dominant deformation in an overall transpressive setting.

Strain paths and strain histories are crucial for the interpretation of the tectonic evolution of a region. Incremental strain studies using syntectonic fibers in pressure shadows provide important information concerning the strain history and have frequently been used to understand the kinematics of deformation (Spencer 1992). We used syntectonic fibers in pressure shadows to determine the incremental and finite-strain patterns in the Gaspé Trough strata. Incremental strain studies have been mostly concerned with fold- and thrust-belts and have usually yielded two-dimensional strain paths confined to planes either parallel or normal to the main tectonic cleavage (Reks & Gray 1983, Beutner & Diegel 1985, Gourlay 1986, Dietrich 1989, Gray & Willman

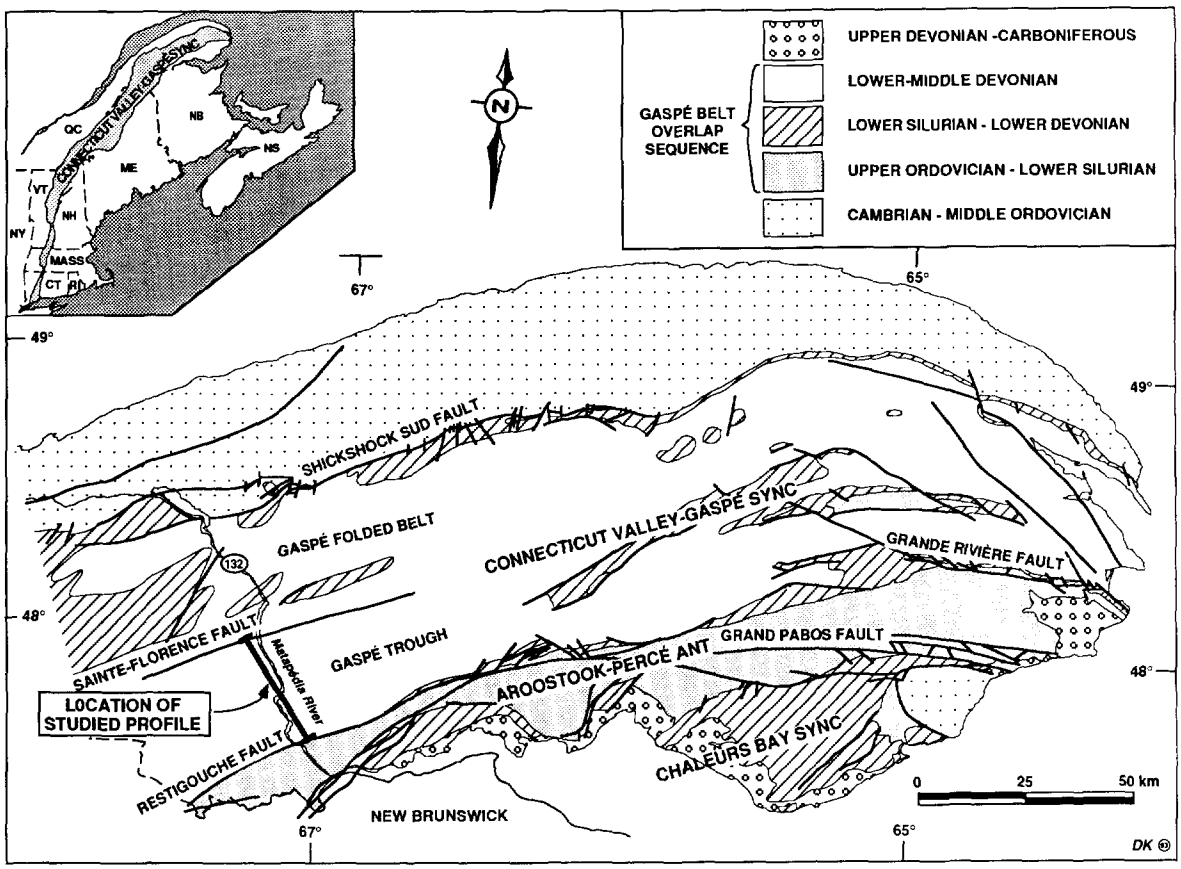

Fig. 1. Geological map of Gaspé Peninsula and location of the studied profile (bottom left). Inset: extent of the Connecticut Valley-Gaspé synclinorium.

1991, Spencer 1992). Our study is unique in that it offers a kinematic analysis of the incremental strain history in three dimensions and quantifies both vertical extension and fold-axis parallel extension. To our knowledge, this is one of the first well documented examples of vertical extension followed by fold-axis parallel extension in a transpressive setting. The sequential development of folds, cleavage and strike-slip faults deduced from fiber geometries in the Gaspé Trough supports the hypothesis that folding initiates before faulting in transpressive terranes.

GEOLOGICAL CONTEXT

In the Gaspé Peninsula, Upper Ordovician to Middle Devonian rocks are part of a single depositional belt, the Gaspé Belt (Bourque *et al.* 1993), an overlap sequence deposited in a successor basin that formed on the destroyed continental margins or relicts of the Iapetus ocean following the Mid- to Late-Ordovician Taconian orogeny (St-Julien & Béland 1982). Rocks of the Gaspé Belt were deformed by the Devonian Acadian orogeny, a major tectonic event in the Canadian Appalachians, and are divided into three major structural zones. These include from north to south the Connecticut Valley-Gaspé synclinorium, the Aroostook-Percé anticlinorium and the Chaleurs Bay synclinorium (Fig. 1). The studied slate belt is part of the Gaspé Belt and is termed the Gaspé Trough, a subdivision of the Connecticut Valley-Gaspé synclinorium (Rodgers 1970).

The Gaspé Trough is composed of slates, siltstones and argillaceous sandstones that underwent Acadian deformation. These sediments belong to the Fortin Group and were deposited by turbidity currents during the early Devonian (Dalton 1987). Rocks of the Fortin Group are part of an extensive series of marine rocks of similar age and lithology extending from the Gaspé Peninsula, westward into New Brunswick and Southeastern Québec, and southward into Maine, New Hampshire and Vermont (Cady 1960, Boucot 1970) (Fig. 1). In the Gaspé, rocks of the Fortin Group yield anchi-metamorphic to lower greenschist grades, and reflectance values suggest temperatures of 330–350°C (Hesse & Dalton 1991).

The Devonian Acadian deformation in this part of the Canadian Appalachians has been the subject of earlier studies (van Staal 1987, Malo & Béland 1989, Malo *et al.* 1992). Major Acadian faults, such as the Grand Pabos, Grande Rivière and Shickshock Sud faults, transect the Gaspé Peninsula (Malo *et al.* 1992) (Fig. 1). The geometry of the fault zones and the shear sense of ductile and brittle fault structures require dextral transcurrent movement along the faults, with displacements on the order of tens to hundreds of kilometers (Malo & Béland 1989, Malo *et al.* 1992). Recent work has established that a dextral transpressive regime is responsible for the

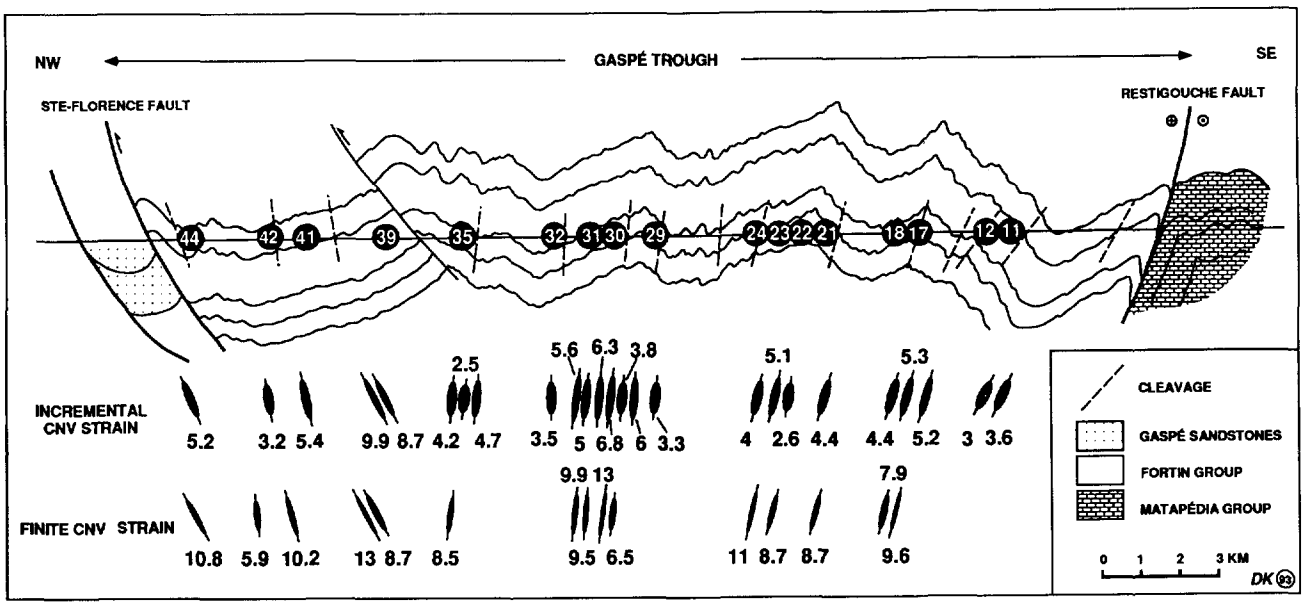

Fig. 2. Structural profile across the Gaspé Trough slate belt based on the outcrop geology along Highway 132 in western Gaspé with incremental and finite CNV strain data (R) and outcrop location; see Fig. 1 for location of the profile. Incremental CNV strain (R) is the shape of the finite strain ellipse in the CNV section after the vertical extension only. Finite CNV strain (R) is the shape of the finite strain ellipse in the CNV section after both extensions, vertical and horizontal.

development of folds and faults within rocks of the Gaspé Belt (Kirkwood & Malo 1993).

Major structural features of the Connecticut Valley-Gaspé synclinorium in western Gaspé are NE-trending upright folds and ENE-trending faults. Folds have wavelengths of 3–5 km and plunge gently towards the northeast or southwest. The studied section along the Matapédia River in western Gaspé is located between two major faults (Fig. 1). Along the northern margin of the Gaspé Trough, rocks of the Fortin Group are juxtaposed against the Lower Devonian Gaspé Sandstones along the Sainte-Florence fault (Fig. 2), interpreted as a reverse fault (Berger 1993). A vertical mineral lineation, SE-dipping cleavage and horizontal mesoscopic fold axes reoriented into a subvertical direction indicate that movement along the Sainte-Florence fault is essentially vertical. To the south, the Restigouche fault separates the Fortin Group from the Upper Ordovician to Lower Silurian limestones of the Matapédia Group within the Aroostook-Percé anticlinorium. The Restigouche fault trends N065° and dips 75° toward the northwest. It extends some 25–30 km eastward to where it merges with the Grand Pabos fault (Fig. 1). Sense of shear indicators along the Restigouche fault indicate dextral oblique slip movement, consistent with its orientation oblique to the Grand Pabos trend (Trudel & Malo 1993).

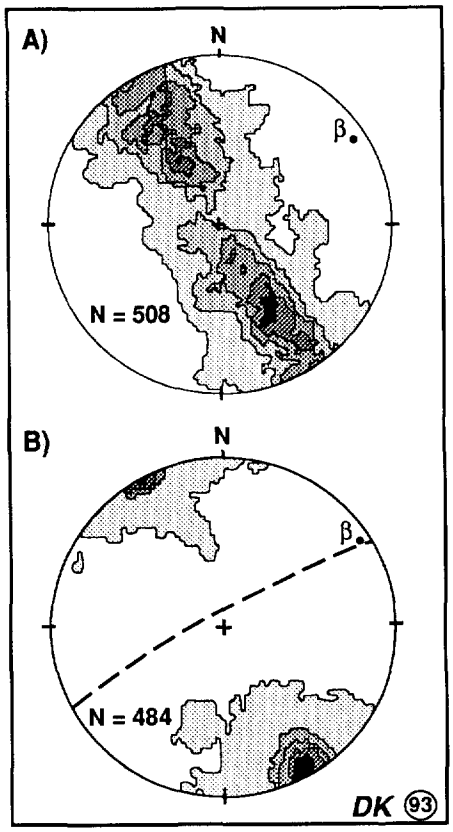

Fig. 3. Contoured structural orientation data for the Fortin Group along the studied section plotted in equal-area hemispherical projection: (a) poles to bedding; contour intervals are 1.5–2.9–4.2–5.6–6.9%; and (b) poles to cleavage; contour intervals are 7–14–21–28–35%.

STRUCTURAL ELEMENTS

Exposure within the Gaspé Trough along the Matapédia River in western Gaspé is very good. Between the Restigouche and Sainte-Florence faults, 12 km of Fortin Group rocks are exposed along a 26 km segment of Highway 132 which follows the Matapédia River. In cross-section, the Gaspé Trough defines a broad anticlinorium (Fig. 2). Regional Acadian folds trend N060° sub-parallel to the structural grain of the Connecticut Valley-Gaspé synclinorium and plunge gently towards the east-northeast (Fig. 3). The folds are open to tight

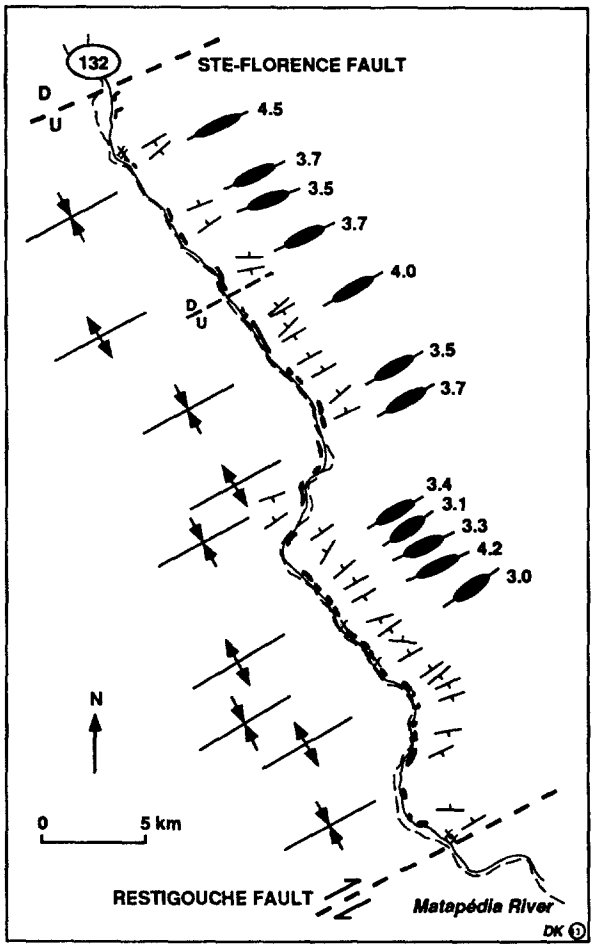

Fig. 4. Map view of the regional incremental CNH strain data (R) variations along the studied profile showing location of major synclines and anticlines; outcrops indicated by black patterns and crosses along Highway 132. The incremental CNH strain (R) is the shape of the finite strain ellipse in the CNH section considering only the horizontal extension.

and have vertical to steeply dipping axial surfaces. Axial surface traces of the major folds are spaced from 2 to 5 km (Fig. 4). Parasitic folds define several orders of folding with lower-order fold wavelengths ranging from 6–40 m and fold amplitudes from 2–5 m (Fig. 5). Abundant quartz veins occur throughout the Fortin Group and usually cut across bedding planes. A well developed cleavage visible in outcrop trends N060° with dips from 75° NW to 75° SE (Fig. 3), parallel to fold axial surfaces. Evidence of dissolution along cleavage planes is shown by truncated quartz grains along cleavage planes. Pressure shadows around pyrite and fibrous quartz–mica overgrowths on detrital quartz grains are evidence for precipitation (see Groshong 1988).

Both reverse and strike-slip faults are recognized along the studied profile. Mesoscopic NE-trending reverse faults, dipping moderately to steeply to the southeast or to the northwest, are geometrically related to the folds (Fig. 5). Displacement along these faults varies from tens of centimeters to a few meters. Strike-slip faults have displacements of a few tens of centimeters. These faults are vertical to subvertical with horizontal slickensides. They crosscut the folded strata and occur sporadically throughout the profile. Dextral and sinistral faults are oriented approximately N100–110° and N160–170°, respectively.

STRAIN ANALYSIS

Pressure shadows

Syntectonic fibers in pressure shadows adjacent to pyrite were used to determine variations in strain across local and regional structures within the slate belt. Incremental strain histories can be determined from syntectonic crystal fibers in pressure shadows (Elliott 1972, Durney & Ramsay 1973, Wickham 1973, Gray & Durney 1979, Ramsay & Huber 1983). Pyrites within rocks of the Fortin Group have diameters that range from 0.02 to 15 mm. Curved fibers occur in pressure shadows around both framboidal and cubic pyrite (Fig. 6a). However, only fibers found around spherical to subspherical framboidal pyrites were used since cubic pyrites are likely to form during tectonic deformation and may not record the full deformation history (Dietrich 1989, Gray & Willman 1991). Other non-spherical pyrites, such as elongate and flattened discoidal pyrites subparallel to bedding, also occur in these rocks. These irregular forms have anomalously long pressure shadows and were not considered in this study. Fibers around the larger pyrites (>1 mm) consist mainly of quartz and calcite whereas fibers around the smaller pyrites (<1 mm) are composed essentially of quartz and chlorite. Fibers show characteristics of antiaxial growth. Some pressure shadows contain small pyrite spherules connected by a fiber to the site from which they were detached indicating that growth sense was towards the host pyrite framboid (Beutner & Diegel 1985) (Fig. 6b).

Fibers were studied in three mutually perpendicular thin sections: cleavage-parallel (CP), cleavage-normal vertical (CNV) and cleavage-normal horizontal (CNH). Figure 7(a) illustrates the position of the sections relative to the orientation of structural elements (folds, cleavage and mineral lineation). The main tectonic cleavage is assumed to approximate the XY plane of the finite strain ellipsoid (Ramsay & Huber 1983). A weakly developed subvertical mineral lineation (L) can be observed at a few locations along the studied profile and was assumed to be parallel to the X direction of the finite strain ellipsoid. True orientation of the finite strain ellipsoid within rocks of the Gaspé Trough is discussed further in a following section.

Fiber orientation

The analysis of fibers within three orthogonal directions is important in order to develop a three-dimensional picture of the orientation of the incremental extensions. Fibers within pressure shadows along the studied cross-section are present in CNV, CNH and CP sections. Individual elongate pyrites are stretched and pulled apart in CNV and CNH planes. Such evidence can be taken to indicate that stretching occurred simul-

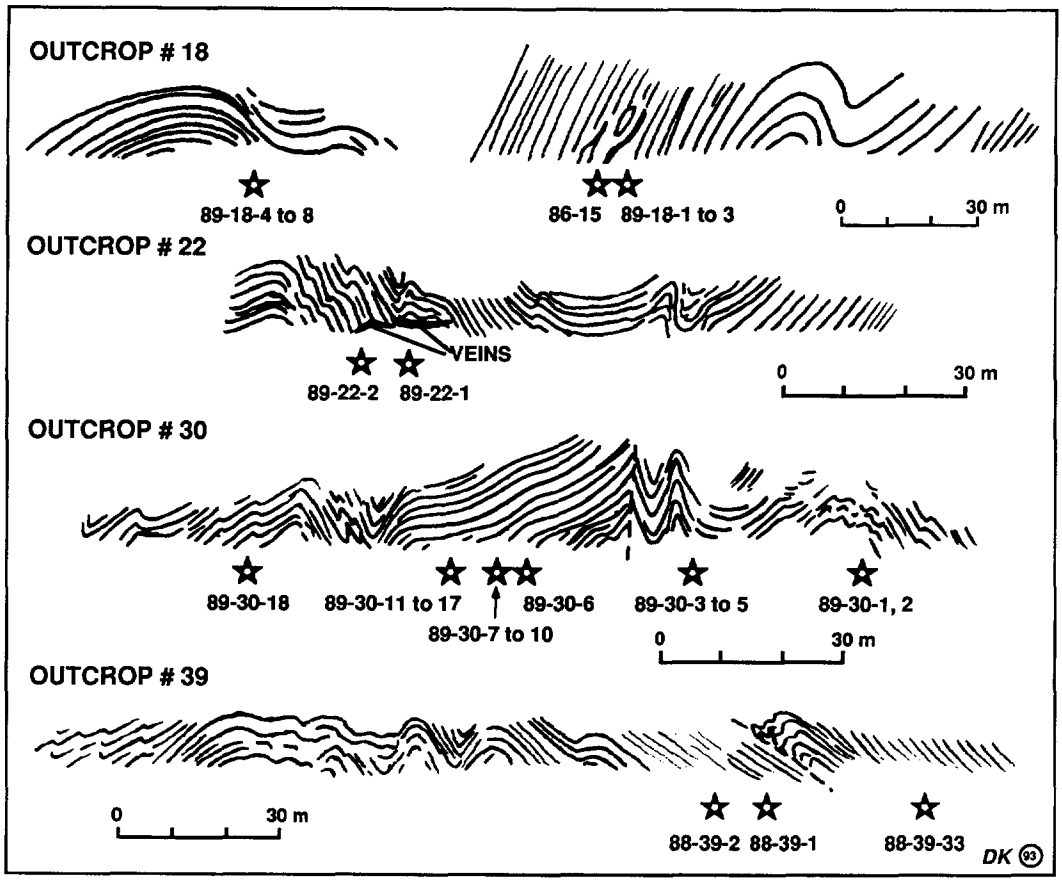

Fig. 5. Line drawings of studied sections showing mesoscopic folds, faults and sample location. See Fig. 2 for location of outcrops.

taneously in more than one direction. However, key aspects of the fiber geometry and their growth within rocks of the Gaspé Trough can be deduced by closely examining the fiber patterns in a chocolate tablet structure developed in a pyrite layer in a CP section and gives an almost complete picture of the incremental strain evolution (Fig. 6c). The antitaxial fibers in Fig. 6(c) show curved forms that point to a changing incremental strain sequence during progressive deformation. The principal extension initiated in a vertical direction, subparallel to X, and rotated in a counter-clockwise sense towards a horizontal direction, subparallel to Y. Thus, fibers in CP planes can be clearly divided into two segments; the first-formed segments are vertical while the youngest part of the fibers are horizontal (Figs. 6c & d). These two fiber segments are perpendicular and can be observed separately in two orthogonal sections, CNV and CNH sections (Fig. 8).

Fiber curvatures

Fiber curvatures are observed in the CNV, CNH and CP sections. Close examination of the older fiber segments observed in the CNV sections show that the fibers initially grew perpendicular to bedding and progressively curved towards the final position of the trace of the cleavage (Figs. 6a & f). Fiber curvatures in CNV sections are divided into two distinct patterns: fibers around pyrites sampled from NW-dipping limbs show clockwise curvatures and fibers from SE-dipping limbs show counter-clockwise curvatures. These curvatures represent rotation of the rock body through a fixed vertical extension direction on oppositely rotating fold limbs (Kirkwood 1993). Although curved fibers generally reflect successive non-coaxial strain increments, the observed curvatures in CNV sections are consistent with successive coaxial strain increments with a vertical maximum stretching direction (Kirkwood in press).

In sections cut through the ends of the larger pyrite grains, the youngest fiber segments, i.e. those closest to the pyrite framboid, curve out of the CNV section plane and the field of view (Figs. 6g & h). Their traces can be followed in the CNH plane where the oldest fiber segments are perpendicular to the thin section and the youngest fiber segments are parallel to the thin section. Almost all fibers display clockwise curvatures in CNH sections (Fig. 8), independent of their position within the folds. Such patterns are related to a clockwise reorientation of the incremental strain axes and reflect the noncoaxiality of this part of the deformation. The fiber geometry observed in CNH sections is consistent with regional dextral shear along major faults, such as the Grand Pabos fault, during the Acadian orogeny (Kirkwood 1993). Within strike-slip zones maximum extension and shortening axes are horizontal and parallel to the major and minor strain ellipse axes, respectively, and both are oblique to the shear direction (Wilcox *et al.* 1973). In the Gaspé, major dextral strike-slip

faults trend roughly N080° and are related to a northwest directed compression during the Acadian orogeny (Malo & Béland 1989). The major axis of the corresponding finite strain ellipse is subhorizontal and oriented northeast, parallel to the regional cleavage. Horizontal extension within rocks of the Gaspé Trough reflects the strain imposed on the rocks during the regional transcurrent simple shear that produced the strike-slip faults. Observed clockwise fiber curvatures in the CNH sections are a direct consequence of the dextral shear along the faults. Rocks located within the southern boundary zone of the Grand Pabos-Restigouche fault in western Gaspé (Matapédia Group, see Fig. 1) also record horizontal extension within the cleavage plane (Kirkwood 1993) which we relate to the same regional transcurrent deformation.

INCREMENTAL STRAIN AND DEFORMATION HISTORY

Strain patterns

The measurement technique chosen was the rigid fiber model outlined by Ramsay & Huber (1983), which assumes that fibers are parallel to the incremental extensions in the rock and that there is no rigid-body rotation between the fibers, pyrite and matrix. Rigid body deformation for pressure shadows in rocks of the Gaspé Trough is indicated by the shape of the pressure shadow boundaries which are identical to the shape of the walls of the pyrite grains (Ramsay & Huber 1983). The rigid fiber method has been used to determine strain in different fold belts (Reks & Gray 1983, Beutner & Diegel 1985, Dietrich 1989, Gray & Willman 1991, Spencer 1992) and has been proven to be quite consistent (Spencer 1991). This method assumes plane strain and constant volume strain. Fiber geometries within rocks of the Gaspé Trough clearly indicate that for each successive increment of the deformation, extension occurred in only one direction parallel to the maximum principal extension (e_1) and that no extension occurred parallel to the intermediate principal extension (e_2). Thus, rocks of the Gaspé Trough in western Gaspé suggest incremental plane strain. Although it is difficult to determine the actual volume change during deformation, we suggest that most of the dissolved material is redeposited locally in the rock system within veins, pressure shadows and overgrowths around pyrite and detrital quartz grains with little or no volume change, as demonstrated in other fold and slate belts (Mitra *et al.* 1984, Beutner & Diegel 1985, Waldron & Sandiford 1988, Protzman & Mitra 1990). Previous work has shown that overgrowths around pyrite and detrital grains are largely lacking where substantial volume loss can be demonstrated (Beutner & Charles 1985).

Total finite strain is obtained by measuring the successive increments of an entire fiber in three dimensions. Such a measurement technique is impossible using two-dimensional thin sections. Thus elongations measured in CNV, CNH and CP planes ($1+e_{i1xz}$, $1+e_{i1yz}$ and $1+e_{i1xy}$, see Fig. 7b) reflect only part of the total elongation and are considered increments of the total strain. Even though some of the pressure shadows display slight curvatures in the older fibers in CP section (see Fig. 6d), the path followed by the fibers throughout the entire deformation is mostly parallel to the CNV (vertical) and CNH (horizontal) sections (Fig. 8), and strain can be divided into two separate, orthogonal two-dimensional sections. Semi-axes of a finite strain ellipsoid resulting from the superposition of two incremental strain ellipsoids can be obtained by multiplying the two sets of semi-axes (Ramsay & Huber 1983). By following the displacement of fibers in time, we were able to obtain the calculated total finite elongations by multiplying the successive total incremental extensions in CNV and CNH sections (Fig. 7c):

$$1+e_{f_1} = (1 + e_{i1xz})(1 + e_{i1yz}).$$

Calculated total finite elongations most probably slightly underestimate the total extension since fibers are not entirely parallel to CNV and CNH sections (see Fig. 6d).

We used 529 measurements from 90 samples at 30 different sites along the profile (Fig. 2) to obtain direct values of the maximum principal extension ($1 + e_{i1}$) in the CP, CNV and CNH sections and to calculate the total strains at individual localities (Appendix Tables A1 and A2). Methods of strain determination are discussed in the Appendix. Strain values in Tables A1 and A2 represent the mean value of the strains determined in thin sections at a given sample site. Incremental strain axial ratios (R_i) determined in the CNV and CNH sections range from 1.7 to 9.8 and 1.3 to 4.5, respectively (Figs. 2 and 4; Tables A1 and A2). Finite strain axial ratios (R_f) vary between 5.9 and 13 (Table 1). Strain can be separated into a vertical component (e_{f1}) and hori-

Fig. 6. (a) Photomicrograph of curved fiber around pyrite framboid as seen in CNV section. S_0: bedding, S_1: cleavage. Sample No. 86-33-2, scale bar is 2 mm. (b) Photomicrograph of small pyrite framboids at the edges of the pressure fringe connected by a fiber to the site from which they were detached. This indicates that growth sense was towards the host pyrite. CNH section, sample No. 89-18-6, scale bar is 1 mm. (c) Photomicrograph of a chocolate tablet structure developed in a pyrite layer, as seen in CP section. The curved form of the fibers show that extension initiated in a direction subparallel to X (vertical) and rotated towards the Y direction (horizontal). Sample No. 89-35-5a, scale bar is 1 mm. (d) Photomicrograph of curved fibers in CP section. First formed fibers are subvertical (parallel to X) and youngest fibers subhorizontal (parallel to Y). Sample No. 89-18-6, scale bar is 0.4 mm. (e) Close-up of the younger, subhorizontal fibers that clearly cut across the older, subvertical fibers. See location of this photomicrograph on photomicrograph (d). (f) Photomicrograph showing the fibers in CNV section which initially grew perpendicular to bedding (S_0) and progressively rotated toward the cleavage (S_1). Sample No. 89-24-1, scale bar is 1 mm. (g) Photomicrograph of youngest fiber segments in CNV section (seen here perpendicular to the section) curving out of section. The observed fibers are attached to the thicker central part of the pyrite grain. Sample No. 89-23-1a, scale bar is 1 mm. (h) Photomicrograph of youngest fiber segments in CNV section (seen here perpendicular to the section) curving out of section. The observed fibers are attached to the thicker central part of the pyrite grain. Sample No. 89-30-12, scale bar is 1 mm.

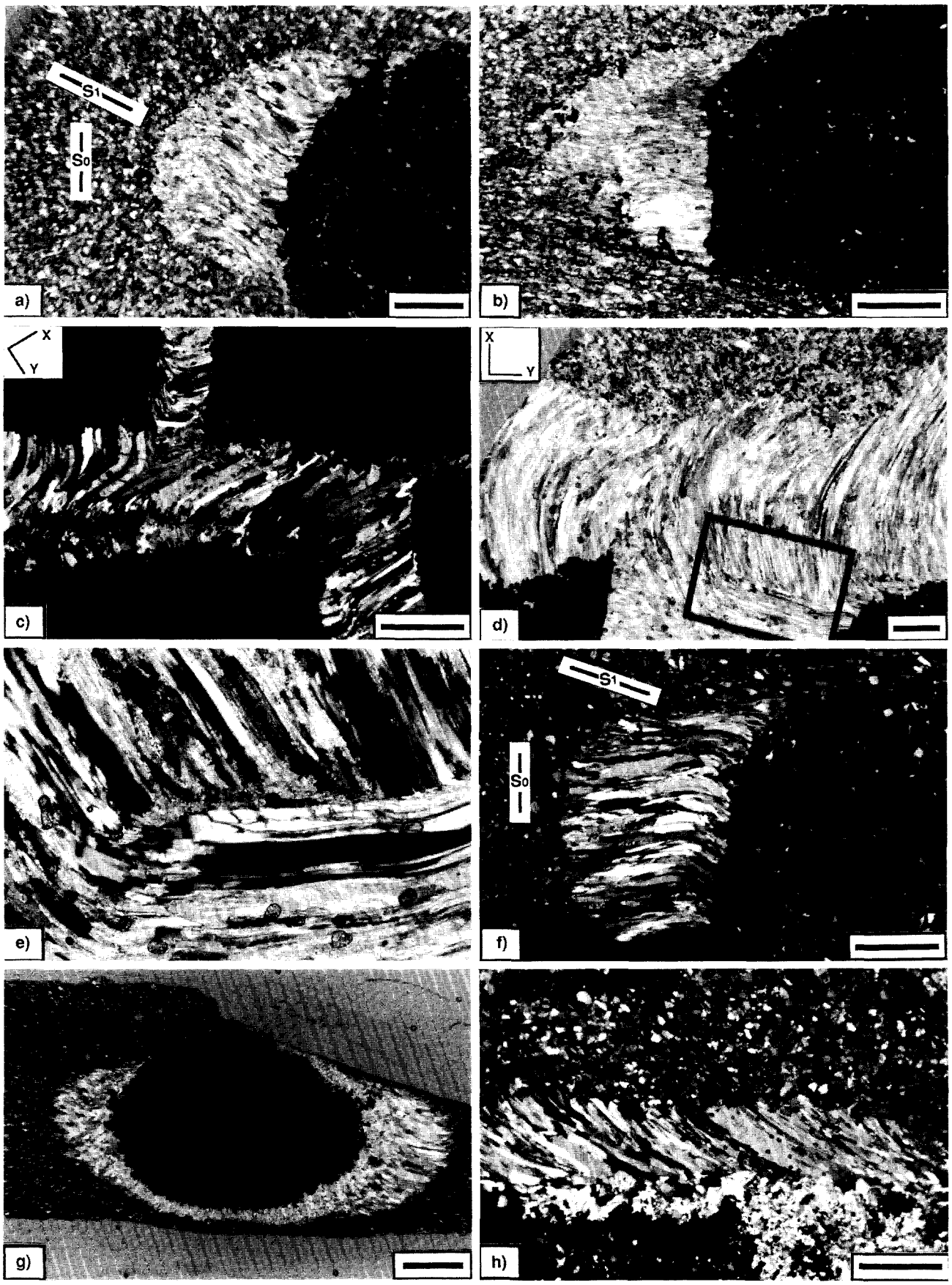

Fig. 6.

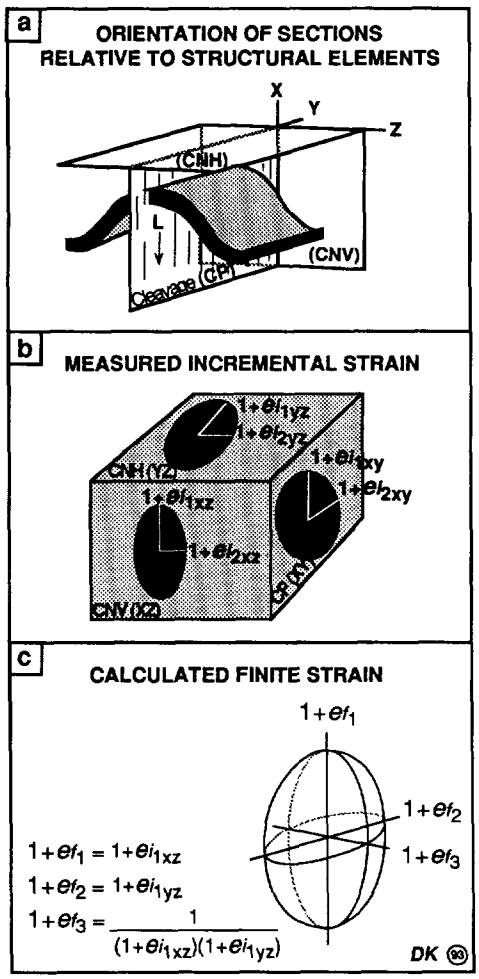

Fig. 7. (a) Orientation of CP, CNV and CNH sections relative to folds, cleavage and mineral lineation (L). (b) Measured incremental elongation in rock samples. The strain ellipses obtained for each of the three sections are incremental strain ellipses. (c) Calculated finite strain. The X and Y axes of the finite strain ellipsoid are given by $(1 + ei_{1xz})$ and $(1 + ei_{1yz})$, respectively. However, the total finite elongation $(1 + e_{f1})$ at each site is obtained by multiplying the two incremental elongations, $(1 + e_{i1xz})$, parallel to X of the finite ellipsoid, and $(1 + ei_{1yz})$, parallel to Y of the finite ellipsoid.

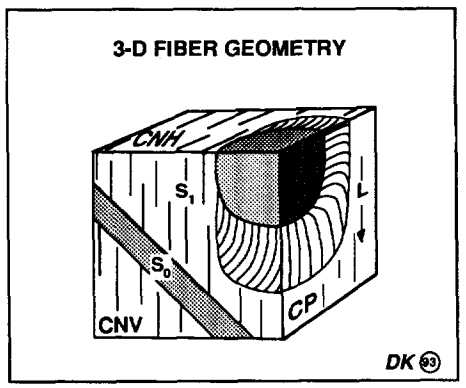

Fig. 8. Three dimensional path of fibers around pyrite located on a SE-dipping limb (outcrop No. 18). Counter-clockwise rotation in the CNV section is followed by rotation in the CP section where fibers are first parallel to X then to Y. Younger fibers in CNH section rotate clockwise. S_0: bedding, S_1: cleavage, L: mineral lineation.

Table 1. Calculated total elongations and finite strain (R)

Outcrop no.	d (km)	$1 + e_{f1}$	$1 + e_{f2}$	$1 + e_{f3}$	R
18	6.490	2.31	1.79	0.24	9.6
18	6.620	2.13	1.73	0.27	7.9
21	8.600	2.09	2.04	0.24	8.7
23	9.760	2.25	1.75	0.26	8.7
24	10.080	2.42	1.84	0.22	11.0
30	13.945	1.87	1.84	0.29	6.4
30	14.010	2.59	1.91	0.20	13.0
31	14.348	2.27	1.80	0.24	9.5
31	14.460	2.37	1.80	0.24	9.9
35	17.915	2.05	2.00	0.24	8.5
39	19.850	2.31	1.36	0.32	7.2
39	19.870	2.59	1.93	0.20	13.0
41	21.800	2.35	1.87	0.23	10.2
42	22.750	1.77	1.91	0.30	5.9
44	24.850	2.27	2.11	0.21	10.8

d = distance north of Restigouche fault

$1 + e_{f1} = 1 + e_{i1xz}$

$1 + e_{f2} = 1 + e_{i1yz}$

$$1 + e_{f3} = \frac{1}{(1 + e_{i1xz})(1 + e_{i1yz})}$$

$$R = \frac{1 + e_{f1}}{1 + e_{f3}}.$$

zontal or fold-axis parallel component (e_{f2}). Vertical extensions range from 77 to 159% and fold-axis parallel extensions range from 36 to 111%. Minimum elongations (e_{f3}) at each site shown in Table 1 were calculated by designating $1+e_{f3}$ as the reciprocal of the maximum finite elongation (Fig. 7c). As such, horizontal shortening across the cleavage varies from 68 to 80% along the slate belt.

There is no apparent correlation between strain and position within mesoscopic folds (limb vs hinge) nor between strain and bedding-cleavage angles, as observed in older fold belts (Beutner & Diegel 1985, Gray & Willman 1991). However, strain magnitude does vary with lithology. Measured maximum extensions are smaller for fibers in sandstones. The lower strains recorded in sandstones can be attributed to the higher competency of these units relative to the argillaceous layers. Cleavage refraction from pelitic layers to sandstone also implies lower strain in the sandstones (Treagus 1983). Regionally, strain estimates are quite uniform and reflect only slightly higher strain in the central part of the anticlinorium and within the hangingwall of a reverse fault located at outcrop No. 29 (Figs. 2 and 5).

Deformation history

Fiber patterns within rocks of the Gaspé Trough clearly indicate that vertical extension was followed by horizontal extension. Similar fiber patterns have been attributed to internal reorientation of strain axes caused by a sudden change in the regional incremental strain history (Gourlay 1986, Dietrich 1989, Spencer 1992). The two major incremental longitudinal extensions observed within rocks of the Gaspé Trough are interpreted as an older strain component responsible for stretching subparallel to the X-direction of the finite strain ellipsoid

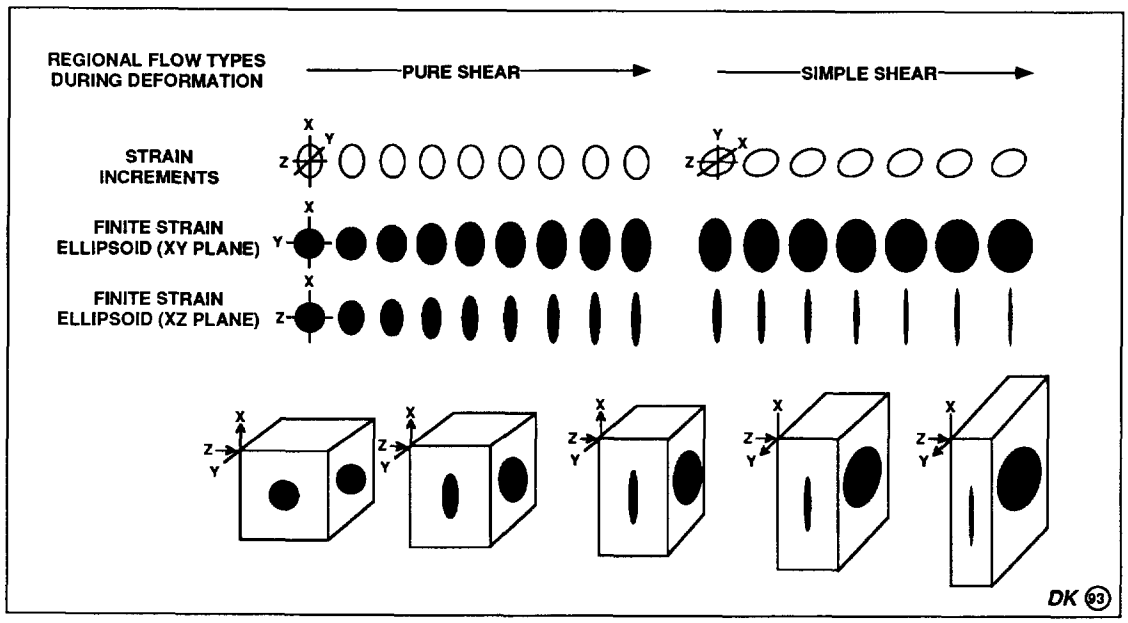

Fig. 9. Representation of finite strain ellipse sequence resulting from the superposition of constant strain increments. Overall flattening deformation within the Gaspé Trough was built up by successive plane strain increments during two major deformational components: (1) coaxial shortening with subvertical stretching; (2) non-coaxial shortening with subhorizontal stretching.

which is vertical followed by a younger strain component responsible for stretching subparallel to the *Y*-direction which is horizontal. Evidence that the two strain events are part of a continuous, progressive deformation is given by the fibers themselves which can be traced continuously through sharp bends from the oldest to the youngest segments (Figs. 6c & d). Also, rocks of the Fortin Group record only one penetrative deformation event, ascribed to the Acadian Orogeny.

The sharp change in fiber orientation indicates a sudden change in the kinematic history of the slate belt. The first component (vertical extension), best recorded in CNV planes, is related to folding and tightening of folds during coaxial deformation (pure shortening) (Kirkwood in press). The younger strain component responsible for horizontal extension is attributed to regional dextral transcurrent shearing. Both components are compatible with a global transpressive setting. It has been shown that rocks bordering fault zones in transpressive systems are affected by both pure and simple shear (Sanderson & Marchini 1984). In such systems, shortening normal to the fault zone and transcurrent shear parallel to the fault zone bring about the development of folds, thrust faults and transcurrent faults. Such a model is consistent with the geology of this part of the Canadian Appalachians. Detailed analysis of deformation fabrics within fault zones in southern Gaspé demonstrated that strike-slip faulting occurred within a dextral transpressive regime (Kirkwood & Malo 1993).

Finite strain ellipsoid

The finite strains within rocks of the Gaspé Trough are of flattening type (e_{f_1} and e_{f_2} positive) as indicated by stretched pyrite in both CNV and CNH sections. The shape of the finite strain ellipsoid depends on the progressive deformation history of the slate belt. Analysis of the incremental strains suggests that the overall flattening deformation recorded by the slates was built up by successive plane strain increments. As previously discussed, the strain history of the slate belt requires two separate deformational components. The strain increments during the first strain event are coaxial and characterized by a maximum incremental *X*-axis oriented subvertically (Fig. 9). This component was followed by an abrupt transition whereby non-coaxial strain increments with *X*-axes oriented horizontally were superposed on the vertically elongated ellipsoid (Fig. 9). However, this late subhorizontal stretch was not strong enough to reorient the positions of the major and minor axes of the finite strain ellipse. Consequently, the maximum finite stretching direction is subvertical and parallel to the observed mineral lineation.

VERTICAL AND FOLD-AXIS PARALLEL EXTENSION IN A TRANSPRESSIVE SETTING

The measured extensions along the studied profile show up to 160% vertical extension followed by up to 110% fold-axis parallel extension. Fold-axis parallel extension has been described elsewhere in a number of fold belts. It has been documented in internal zones of collisional orogens formed by oblique continental subduction (Ellis & Watkinson 1987) as well as in rocks deformed within transpressional regimes (Bürgmann 1991). Stretching histories similar to the one defined within rocks of the Gaspé Trough, i.e. extension orthogonal to fold axes followed by extension parallel to fold

axes, has been recorded in fold- and thrust-belts and has been attributed to a change in the direction of shear within the thrust nappes (Merle & Brun 1984, Gourlay 1986, Dietrich 1989, Spencer 1992).

The regional structural history within this part of the Canadian Appalachian orogen, i.e. the Gaspé and northern New Brunswick, involves dextral transpression culminating in major strike-slip faulting during the Acadian deformation (Kirkwood & Malo 1993, de Roo & van Staal 1994). Transpression is now being recognized as very significant in the kinematics of collisional orogens, especially where oblique convergence is involved (Bürgmann 1991, Cobbold *et al.* 1991, Fielitz 1992). The spatial partitioning of strain within transpressive settings between strike-parallel and strike-normal components is now well documented in many regions (see Platt 1993). The incremental strain history recorded by syntectonic fibers in the Gaspé Trough documents the progressive deformation history of the slate belt and shows that strain is also partitioned in time within this transpressive setting. Growth patterns of the fibers in the slate belt clearly prove that folding resulted from coaxial deformation during the first stages of the deformation. The folding was followed by development of the cleavage in the final state (Kirkwood 1993). During this first part of the deformation, the extension was vertical and the pure-shear component of the transpressive deformation was predominant. Strain estimates indicate shortening during this part of the deformation accounts for approximately 70% of the total shortening (Kirkwood in press). The second strain component brought about fold-axis parallel extension which we relate to the map-view simple shear component of the transpressive regime. The abrupt reorientation of the extension direction from subvertical to subhorizontal records the transition from a pure shortening deformation to a simple shear dominant deformation within the overall transpressive setting. The strain recorded during the last stage of the deformation (30% of the total shortening) contributed to further tightening of the folds (Kirkwood 1993). Alternatively, our data set cannot rule out the fact that the first part of the deformation might reflect a purely convergent setting that evolved into a transpressive setting during oblique convergence.

A discussion on the plate tectonic models of the Canadian Appalachians is beyond the scope of this paper. However, one must concede that the abrupt reorientation of the maximum extension within rocks of the Gaspé Trough reflects a change in kinematics in this part of the orogen during the Mid-Devonian Acadian orogeny. Many other collisional orogens exhibit two distinct deformation phases. As pointed out above, stretching lineations show curved patterns in arcuate fold- and thrust-belts and display more than one stretching direction. In many orogens, stretching lineations trend at high angles to the mountain belt in the external parts of the orogen whereas strike-parallel stretching lineations are more common in the internal parts of the orogen (Platt *et al.* 1989). In frontal regions of forearcs, the geometry and the mechanical properties of the thrust wedge will influence the distribution of the strike-parallel component of velocity in an obliquely convergent system (Platt 1993). In the Northern Appalachians, the Acadian orogeny resulted from oblique convergence between composite Laurentia and the Gander margin of Gondwana during Late Silurian–Middle Devonian times (Rast & Skehan 1993, de Roo & van Staal 1994). Thus, orogen-perpendicular extension in the external zone and orogen-parallel extension in the internal zone of the Acadian orogen are to be expected. The first stage structures documented in the Gaspé Trough which record vertical stretching and orogen-perpendicular shortening were most probably formed while the slate belt was located within the most external part of the orogen. As the locus of intense deformation migrated towards the foreland, the position of the slate belt evolved within the mountain belt, and the distance separating it from the internal part of the orogen was reduced. Consequent modifications of the geometrical and mechanical properties within the slate belt could have caused the development of structures more typical of the internal parts of orogens, such as fold-axis parallel extension and strike-slip faulting. The abrupt reorientation of the strain principal directions recorded by the fibers within the Gaspé Trough is very convincing evidence in support of such a kinematic transition in the foreland. However, the overall structural style of the belt is characteristic of external parts of orogens, the Gaspé Trough being included in the external zone of the Acadian orogen.

CONCLUSIONS

Syntectonic fibers in pressure shadows around pyrite in the studied slate belt provide a unique three-dimensional record of the incremental strain history within a convergent wrench setting. Close examination of the fibers shows that they first curved towards parallelism with the cleavage within vertical sections normal to the cleavage and then rotated from a vertical X-parallel orientation to an essentially horizontal Y-parallel orientation in cleavage parallel sections. Up to 160% vertical and 110% fold-axis parallel extensions were recorded in the folded sequence and an overall regional shortening of up to 80% is estimated for the slate belt in western Gaspé. Considerable fold-axis parallel extension is a result of the map-view simple shear component of the transpressive regime. This incremental strain study clearly demonstrates the kinematic transition from a pure shortening deformation to a simple shear dominant deformation in an overall transpressive setting. Folding, cleavage development, fold-axis parallel extension and strike-slip faulting are all related to the same progressive deformation attributed to continued plate convergence and culminating in collision during the Acadian Orogeny.

Acknowledgements—Financial assistance was received from the Fonds pour la formation de chercheurs et l'aide à la recherche (FCAR) through a Team Grant to P. A. Bourque, the Natural Sciences and Engineering Research Council of Canada (NSERC) through an oper-

ating grant (GP1908) to M. Malo. D. Kirkwood was supported by NSERC and le Fonds pour la formation de chercheurs et l'aide à la recherche (FCAR). Comments and suggestions from E. C. Beutner were deeply appreciated and greatly improved the quality of this contribution. We thank Steven Wojtal and two anonymous referees for their critical review of the manuscript.

REFERENCES

Berger, J. 1993. Etude structurale et gîtologique de la faille de Sainte-Florence: Gaspésie. *Ministère de l'Energie et des Ressources du Québec*, **MB 93-01**.

Beutner, E. C. & Charles, E. G. 1985. Large volume loss during cleavage formation, Hamburg sequence, Pennsylvania. *Geology* **13**, 803–805.

Beutner, E. C. & Diegel, F. 1985. Determination of fold kinematics from syntectonic fibers in pressure shadows, Martinsburg Slate, New Jersey. *Am. J. Sci.* **285**, 16–50.

Boucot, A. J. 1970. Devonian slate problems in the Northern Appalachians. *Bull. geol. Surv. Maine* **23**, 42–48.

Bourque, P. A., Gosselin, C., Kirkwood, D., Malo, M. & St-Julien, P. 1993. Le Silurien du segment appalachien Gaspésie-Matapédia-Témiscouata, Québec: stratigraphie, géologie structurale et paléogéographie (Rapport final). *Ministère de l'Energie et des Ressources du Québec* **MM 93-25**.

Bürgmann, R. 1991. Transpression along the southern San Andreas fault, Durmid Hill, California. *Tectonics* **10**, 1152–1163.

Cady, W. M. 1960. Stratigraphic and geotectonic relationships in northern Vermont and southern Québec. *Bull. geol. Soc. Am.* **71**, 531–576.

Cobbold, P. R., Gapais, D. & Rossello, E. A. 1991. Partitioning of transpressive motions within a sigmoidal foldbelt: the Variscan Sierra Australes, Argentina. *J. Struct. Geol.* **13**, 743–758.

Dalton, E. 1987. Sedimentary facies and diagenesis of the Lower Devonian Temiscouata and Fortin formations, Northern Appalachians, Québec and New Brunswick. Unpubl. M.Sc. Thesis, McGill University, Montréal.

de Roo, J. A. & van Staal, C. R. 1994. Transpression and extensional collapse; steep belts and flat belts in the Appalachian Central Mobile Belt, northern New Brunswick, Canada. *Bull. Geol. Soc. Am.* **106**, 541–552.

Dietrich, D. 1989. Fold-axis parallel extension in a arcuate fold- and thrust belt: the case of the Helvetic nappes. *Tectonophysics* **170**, 183–212.

Durney, D. W. & Ramsay, J. G. 1973. Incremental strains measured by syntectonic crystal growth. In: *Gravity and Tectonics* (edited by DeJong, K. & Scholten, R.). Wiley, New York, 67–96.

Elliott, D. 1972. Deformation paths in structural geology. *Bull. Geol. Soc. Am.* **83**, 2621–2638.

Ellis, M. A. & Watkinson, A. J. 1987. Orogen-parallel extension and oblique tectonics: the relation between stretching lineations and relative plate motions. *Geology* **15**, 1022–1026.

Fielitz, W. 1992. Variscan transpressive inversion in the northwestern central Rhenohercynian belt of western Germany. *J. Struct. Geol.* **14**, 547–563.

Gourlay, P. 1986. La déformation du socle et des couvertures delphino-helvétiques dans la région du Mont Blanc (Alpes occidentales). *Bull. Soc. geol. Fr.* **8**, 159–169.

Gray, D. R. & Durney, D. W. 1979. Investigations on the mechanical significance of crenulation cleavage. *Tectonophysics* **58**, 35–79.

Gray, D. R. & Willman, C. E. 1991. Thrust-related strain gradients and thrusting mechanisms in a chevron-folded sequence, southeastern Australia. *J. Struct. Geol.* **13**, 691–710.

Groshong, R. H. 1988. Low-temperature deformation mechanisms and their interpretation. *Bull. geol. Soc. Am.* **100**, 1329–1360.

Hesse, R. & Dalton, E. 1991. Diagenetic and low-grade metamorphic terranes of Gaspé Peninsula related to the geological structure of the Taconian and Acadian orogenic belts, Québec Appalachians. *J. Met. Geol.* **9**, 775–790.

Jamison, W. R. 1991. Kinematics of compressional fold development in convergent wrench terranes. *Tectonophysics* **190**, 209–232.

Kirkwood, D. 1993. Étude qualitative et quantitative de la déformation acadienne du bassin siluro-dévonien de la péninsule gaspésienne, Appalaches du Nord. Ph.D. thesis, Université Laval, Québec, Canada.

Kirkwood, D. In press. Strain partitioning and progressive deformation history in a transpressive belt, northern Appalachians. *Tectonophysics*.

Kirkwood, D. & Malo, M. 1993. Across-strike geometry of the Grand Pabos fault zone: evidence for Devonian dextral transpression in the Québec Appalachians. *Can. J. Earth Sci.* **30**, 1363–1373.

Lafrance, B. 1989. Structural evolution of a transpression zone in north central Newfoundland. *J. Struct. Geol.* **11**, 705–716.

Malo, M. & Béland, J. 1989. Acadian strike-slip tectonics in the Gaspé Region, Québec Appalachians. *Can. J. Earth Sci.* **26**, 1764–1777.

Malo, M., Kirkwood, D., DeBroucker, G. & St-Julien, P. 1992. A re-evaluation of the position of the Baie Verte-Brompton Line in the Québec Appalachians: the influence of mid-Devonian strike-slip faulting in Gaspé Peninsula. *Can. J. Earth Sci.* **29**, 1265–1273.

Merle, O. & Brun, J. P. 1984. The curved translation of the Parpaillon Nappe (French Alps). *J. Struct. Geol.* **6**, 711–719.

Mitra, G., Yonkee, W. A. & Gentry, D. J. 1984. Solution cleavage and its relationship to major structures in the Idaho–Utah–Wyoming thrust belt. *Geology* **12**, 354–358.

Platt, J. P. 1993. Mechanics of oblique convergence. *J. Geophys. Res.* **98**, 16,239–16,256.

Platt, J. P., Behrmann, J. H., Cunningham, P. C., Dewey, J. F., Helman, M., Parish, M., Shepley, M. G., Wallis, S. & Weston, P. J. 1989. Kinematics of the Alpine arc and the motion history of Adria. *Nature* **337**, 158–161.

Protzman, G. M. & Mitra, G. 1990. Strain fabric associated with the Meade thrust sheet: implications for cross-section balancing. *J. Struct. Geol.* **12**, 403–417.

Ramsay, J. G. & Huber, M. 1983. *The Techniques of Modern Structural Geology*. 1: *Strain Analysis*. Academic Press, London.

Rast, N. & Skehan, J. W. 1993. Mid-Paleozoic orogenesisi in the North Atlantic: the Acadian orogeny. In: *The Acadian Orogeny: Recent Studies in New England, Maritime Canada, and The Autochthonous Foreland* (edited by Roy, D. C. & Skehan, J. W.). *Spec. Pap. geol. Soc. Am.* **275**, 1–25.

Reks, I. J. & Gray, D. R. 1983. Strain patterns and shortening in a folded thrust sheet: an example from the Southern Appalachians. *Tectonophysics* **93**, 99–128.

Richard, P., Mocquet, B. & Cobbold, P. R. 1991. Experiments on simultaneous faulting and folding above a basement wrench fault. *Tectonophysics* **188**, 133–141.

Rodgers, J. 1970. *The Tectonics of the Appalachians*. John Wiley & Sons Inc, New York.

Sanderson, D. J. & Marchini, W. R. D. 1984. Transpression. *J. Struct. Geol.* **6**, 449–458.

Spencer, S. 1991. The use of syntectonic fibers to determine strain estimates and deformation paths: an appraisal. *Tectonophysics* **194**, 13–34.

Spencer, S. 1992. A kinematic analysis incorporating incremental strain data for the Frontal Pennine Zones of the western French Alps. *Tectonophysics* **206**, 285–305.

St-Julien, P. & Béland, J. 1982. Introduction. In: *Major Structural Zones and Faults of The Northern Appalachians* (edited by St-Julien, P. & Béland, J.). *Spec. Pap. geol. Ass. Can.* **24**, 1–11.

Treagus, S. H. 1983. A theory of finite strain variation through contrasting layers, and its bearing on cleavage refraction. *J. Struct. Geol.* **5**, 351–368.

Trudel, C. & Malo, M. 1993. Analyses des contraintes par méthodes graphiques dans une zone de coulissage: exemple de la région de Matapédia, Gaspésie, Appalaches du Québec. *Can. J. Earth Sci.* **30**, 591–602.

van Staal, C. R. 1987. Tectonic setting of the Tetagouche Group in northern New-Brunswick: Implications for plate tectonic models of the northern Appalachians. *Can. J. Earth Sci.* **24**, 1329–1351.

Waldron, H. M. & Sandiford, M. 1988. Deformation volume and cleavage development in metasedimentary rocks from the Ballarat slate belt. *J. Struct. Geol.* **10**, 53–62.

Wickham, J. S. 1973. An estimate of strain increment in a naturally deformed carbonate rock. *Am. J. Sci.* **273**, 23–47.

Wilcox, R. E., Harding, T. P. & Seely, D. R. 1973. Basic wrench tectonics. *Bull. Am. Ass. Petrol. Geol.* **57**, 74–96.

APPENDIX

Strain determination

The principal incremental extensions were calculated using the rigid fiber model outlined by Ramsay & Huber (1983). Line segments were

constructed along central fibers to define the length of fiber increments. These segments and the center of the pyrite framboid were digitized with the cleavage orientation in the final state as the reference orientation for CNV (XZ) and CNH (YZ) sections, and the vertical as the reference orientation for CP (XY) sections. Coordinates were converted into incremental elongations and corresponding orientations using a computer program written by P. Therrien. Incremental strains and orientations were assembled into incremental strain matrices using a second program written by P. Therrien which computes the progressive finite strains ($1 + e_1$ and $1 + e_2$) and their orientation, assuming plane strain and no volume change i.e. $e_{2_n} = 0$ and $e_{3_n} = 1/(1 + e_{1_n})$ as discussed in the text.

Table A1. Measured incremental strain
Small fringes (<5mm)

CNV sections

No	d(km)	n	$1 + e_{i1xz}$	$1 + e_{i2xz}$	$1 + e_{i3xz}$	$R = (1 + e_1)/(1 + e_3)$
8611*xz*	3.950	7	1.90		0.53	3.6
8612*xz*	4.050	5	1.72		0.58	3.0
8917*xz*	6.250	7	2.29		0.44	5.2
8918-3*xz*	6.490	2	2.31		0.43	5.4
8918-4*xz*	6.620	4	2.05		0.49	4.2
8918-6*xz*	6.620	1	2.60		0.38	6.8
8918-8*xz*	6.620	4	2.09		0.48	4.4
	Mean 6.62		2.13		0.47	4.5
8921-2*xz*	8.600	8	2.09		0.48	4.4
8923*xz*	9.640	2	1.62		0.62	2.6
8923-1*xz*	9.760	1	1.54		0.65	2.4
8923-2*xz*	9.760	4	2.53		0.40	6.3
8923-4*xz*	9.760	1	1.85		0.54	3.4
	Mean 9.76		2.25		0.44	5.1
8924-1*xz*	10.080	7	2.42		0.41	5.9
8924-2*axz*	10.025	4	1.79		0.56	3.2
8924-2*bxz*	10.025	6	2.17		0.46	4.7
8924-2*cxz*	10.025	4	1.91		0.52	3.7
8924-2*xz*	10.025	4	1.86		0.54	3.4
8924-3*xz*	10.025	2	2.18		0.46	4.7
8924-4*xz*	10.025	4	2.19		0.46	4.8
	Mean 10.025		2.02		0.50	4.0
8929*xz*	12.900	4	1.81		0.55	3.3
8930-1*xz*	13.885	5	2.46		0.41	6.0
8930-3*xz*	13.945	6	1.90		0.53	3.6
8930-5*xz*	13.945	10	1.71		0.58	2.9
8930-5*axz*	13.945	9	1.79		0.56	3.2
8930-5*bxz*2	13.945	7	2.14		0.47	4.6
	Mean 13.945		1.87		0.53	3.5
8930-8*xz*	14.010	17	2.57		0.39	6.6
8930-10*xz*	14.010	11	2.62		0.38	6.9
	Mean 14.01		2.59		0.39	6.6
8930-12*xz*	14.030	4	1.82		0.55	3.3
8930-16*axz*	14.030	4	2.25		0.44	5.1
8930-16*bxz*	14.030	7	2.70		0.37	7.3
	Mean 14.03		2.26		0.44	5.1
8931-3*xz*	14.348	1	3.00		0.33	9.1
8931-4*xz*	14.348	5	2.59		0.39	6.6
8931-5*xz*	14.348	9	2.30		0.43	5.3
8931-6*xz*	14.348	3	2.41		0.41	5.9
8931-7*xz*	14.348	10	2.05		0.49	4.2
8931-8*xz*	14.348	1	1.60		0.63	2.5
	Mean 14.348		2.27		0.44	5.2
8931-9*xz*3	14.357	1	2.43		0.41	5.9
8931-10*axz*	14.357	4	2.18		0.46	4.7
8931-10*bxz*	14.357	4	1.87		0.53	3.5
8931-10*cxz*	14.357	1	2.18		0.46	4.7
8931-12*xz*	14.357	4	1.94		0.52	3.7
	Mean 14.357		2.03		0.49	4.1
8931-14*xz*	14.425	3	2.65		0.38	7.0
8931-15*xz*	14.460	4	2.57		0.39	6.6
8931-15*bxz*	14.460	5	2.20		0.45	4.9
	Mean 14.46		2.37		0.42	5.6
8832-2*xz*	15.480	5	1.87		0.53	3.5
8935-1*xz*	17.335	7	2.11		0.47	4.5
8935-3*xz*	17.335	3	2.32		0.43	5.4
	Mean 17.335		2.17		0.46	4.7
8935-5*axz*	17.680	3	1.65		0.61	2.7
8935-5*cxz*	17.680	1	1.32		0.76	1.7
	Mean 17.68		1.57		0.64	2.5
8935-6*xz*	17.915	6	1.67		0.60	2.8
8935-7*xz*	17.915	4	2.03		0.49	4.1
8935-8*cxz*	17.915	5	2.02		0.50	4.0
8935-9*bxz*	17.915	6	2.01		0.50	4.0
8935-9*cxz*	17.915	11	2.30		0.43	5.3
	Mean 17.915		2.05		0.49	4.2

Continued

Table A1. *Continued*

CNH sections

No	d(km)	n	$1 + e_{i1xz}$	$1 + e_{i2xz}$	$1 + e_{i3xz}$	$R = (1 + e_1)/(1 + e_3)$
8839-1*xz*	19.850	5	2.31		0.43	5.4
8839-2*xz*	19.870	6	2.59		0.39	6.6
8841-1*xz*	21.800	6	2.35		0.43	5.5
8842-1*xz*	22.750	4	1.77		0.56	3.2
8844-2*xz*	24.850	3	2.27		0.44	5.2
8918-2*yz*	6.490	4	1.79		0.56	3.2
8918-7*yz*	6.620	8	1.69		0.59	2.9
8918-8*yz*	6.620	6	1.77		0.56	3.2
	Mean 6.62		1.73		0.58	3.0
8921-1*yz*	8.600	9	2.04		0.49	4.2
8922-1*yz*	9.060	7	1.82		0.55	3.3
8922-2*yz*	9.080	4	1.79		0.56	3.2
8923-4*yz*	9.760	10	1.75		0.57	3.1
8924-1*yz*	10.080	7	1.84		0.54	3.4
8930-3*ayz*	13.945	2	1.83		0.55	3.3
8930-3*byz*	13.945	6	1.85		0.54	3.4
8930-7*yz*	14.010	1	1.77		0.56	3.2
8930-8*yz*	14.010	3	1.61		0.62	2.6
8930-10*yz*	14.010	8	2.04		0.49	4.2
	Mean 14.01		1.91		0.52	3.7
8931-6*yz*	14.348	5	1.87		0.53	3.5
8931-15*yz*	14.460	5	2.05		0.49	4.2
8935-7*yz*	17.915	1	1.93		0.52	3.7
8935-9*byz*	17.915	1	2.06		0.49	4.2
	Mean 17.915		2.00		0.50	4.0
8839-1*yz*	19.850	3	1.36		0.74	1.8
8839-2*yz*	19.870	6	1.93		0.52	3.7
8841-1*yz*	21.800	3	1.87		0.53	3.5
8842-1*yz*	24.850	5	2.11		0.47	4.5

CP sections

No	d(km)	n	$1 + e_{i1xy}$	$1 + e_{i2xy}$	$1 + e_{i3xy}$	$R = (1 + e_1)/(1 + e_3)$
8611*xy*	3.950	11	2.55	1.16	0.34	7.5
8612*xy*	4.050	10	2.17	1.29	0.36	6.0
8918-6*axy*	6.620	1	1.80	1.14	0.49	3.7
8923*xy*	9.640	1	1.76	1.10	0.52	3.4
8924-1*xy*	10.080	3	1.89	1.30	0.41	4.6
8924-4*xy*	10.025	2	2.04	1.14	0.43	4.7
8929*xy*	12.900	4	1.84	1.37	0.40	4.6
8930-5*xy*	13.945	7	2.12	1.13	0.42	5.0
8930-8*xy*	14.010	5	3.59	1.25	0.22	16.3
8930-10*xy*	14.010	7	2.78	1.25	0.29	9.6
	Mean 14.01		3.11		0.32	9.7
8931-8*xy*	14.348	2	1.64	1.27	0.48	3.4
8931-10*axy*	14.357	5	2.06	1.24	0.39	5.3
8931-10*bxy*	14.357	2	2.46	1.24	0.33	7.5
	Mean 14.357		2.06	1.25	0.40	5.2
8931-15*xy*	14.460	5	2.04	1.23	0.40	5.1
8935-6*axy*	17.915	4	2.33	1.13	0.38	6.1
8935-6*bxy*	17.915	2	2.03	1.11	0.44	4.6
8935-7*xy*	17.915	1	1.69	1.11	0.53	3.2
	Mean 17.915		2.15	1.09	0.43	5.0

No: thin section number.
d(km): distance from Restigouche fault.
n: Number of fibers around different pyrite framboids measured.

Table A2. Measured incremental strain

Large fringes (>5mm)

CNV sections

No	d(km)	n	$1 + e_{i1xz}$	$1 + e_{i2xz}$	$1 + e_{i3xz}$	$R = (1 + e_1)/(1 + e_3)$
8629*xz*	12.250	3	1.68		0.60	2.8
8632-1*xz*	15.440	2	1.93		0.52	3.7
8918-3*xz*	6.490	1	1.58		0.63	2.5
8918-4*xz*	6.620	1	2.05		0.49	4.2
8918-6*xz*	6.620	1	1.57		0.64	2.5
	Mean 6.62		1.81		0.55	3.3
8923-1*axz*	9.760	1	1.67		0.60	2.8
8923-2*xz*	9.760	2	1.73		0.58	3.0
8924-1*xz*	10.080	1	2.01		0.50	4.0
8924-2*xz*	10.025	2	1.60		0.63	2.5
8930-12*xz*	14.030	1	2.45		0.41	6.0
8930-16*xz*	14.030	2	1.43		0.70	2.0
8931-3*xz*	14.348	1	1.83		0.55	3.3
8931-4*xz*	14.348	1	2.93		0.34	8.6
8931-5*xz*	14.348	1	3.13		0.32	9.8
8931-6*xz*	14.348	1	2.96		0.34	8.7
8931-7*xz*	14.348	1	1.82		0.55	3.3
8931-8*xz*	14.348	1	1.82		0.55	3.3
	Mean 14.348		2.42		0.41	5.9
8931-10*axz*	14.357	1	2.10		0.48	4.4
8931-14*xz*	14.425	1	1.85		0.54	3.4
8935-5*bxz*	17.680	1	1.65		0.61	2.7
8935-8*cxz*	17.680	1	1.93		0.52	3.7
8935-9*cxz*	17.680	1	1.48		0.68	2.2
	Mean 17.68		1.69		0.59	2.9

CP sections

No	d(km)	n	$1 + e_{i1xy}$	$1 + e_{i2xy}$	$1 + e_{i3xy}$	$R = (1 + e_1)/(1 + e_3)$
8629*xy*	12.250	1	1.54	1.10	0.59	2.6
8632*xy*	15.440	1	1.73	1.15	0.50	3.5
8918-6*axy*	6.620	1	1.34	1.18	0.63	2.1
8930-5*xy*	13.945	1	1.33	1.13	0.67	2.0
8930-10*axy*	13.945	1	1.31	1.24	0.62	2.1
8931-10*axy*	14.357	1	1.31	1.24	0.62	2.1
8935-5*axy*	17.680	1	1.42	1.04	0.68	2.1
8935-6*bxy*	17.680	1	1.36	1.04	0.71	1.9
	Mean 17.68		1.39	1.04	0.69	2.0

CNH sections

No	d(km)	n	$1 + e_{i1yz}$	$1 + e_{i2yz}$	$1 + e_{i3yz}$	$R = (1 + e_1)/(1 + e_3)$
8918-2*yz*	6.490	2	1.34		0.75	1.8
8918-6*yz*	6.620	1	1.37		0.73	1.9
8931-10*yz*	14.357	1	1.12		0.89	1.3

No: thin section number.
d(km): distance from Restigouche fault.
n: number of fibers around different pyrite framboids measured.